JOURNAL OF NATURAL PRODUCTS

pubs.acs.org/jnp

Article

Combining Activity Profiling with Advanced Annotation to Accelerate the Discovery of Natural Products Targeting Oncogenic Signaling in Melanoma

Tanja Hell,[‡] Adriano Rutz,[‡] Lara Dürr, Maciej Dobrzyński, Jakob K. Reinhardt, Timo Lehner, Morris Keller, Anika John, Mahabir Gupta, Olivier Pertz, Matthias Hamburger, Jean-Luc Wolfender, and Eliane Garo*

Cite This: https://doi.org/10.1021/acs.jnatprod.2c00146

Read Online

ACCESS | Metrics & More | Article Recommendations | Supporting Information

ABSTRACT: The discovery of bioactive natural products remains a time-consuming and challenging task. The ability to link high-confidence metabolite annotations in crude extracts with activity would be highly beneficial to the drug discovery process. To address this challenge, HPLC-based activity profiling and advanced UHPLC-HRMS/MS metabolite profiling for annotation were combined to leverage the information obtained from both approaches on a crude extract scaled down to the submilligram level. This strategy was applied to a subset of an extract library screening aiming to identify natural products inhibiting oncogenic signaling in melanoma. Advanced annotation and data organization enabled the identification of compounds that were likely responsible for the activity in the extracts. These compounds belonged to two different natural product scaffolds, namely, brevipolides from a *Hyptis brevipes* extract and methoxylated flavonoids identified in three different extracts of *Hyptis* and *Artemisia* spp. Targeted isolation of these prioritized compounds led to five brevipolides and seven methoxylated flavonoids. Brevipolide A (**1**) and 6-methoxytricin (**9**) were the most potent compounds from each chemical class and displayed AKT activity inhibition with an IC_{50} of 17.6 ± 1.6 and 4.9 ± 0.2 μM, respectively.

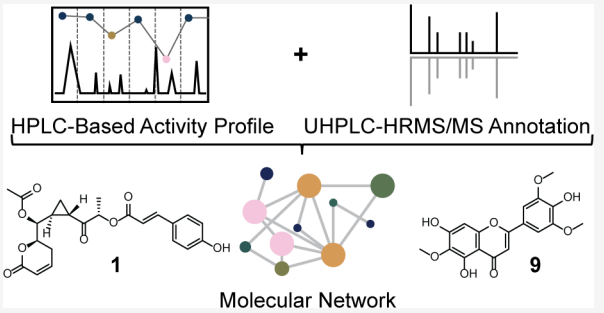

Natural products are a prolific source of new drugs. However, the path from an active extract of an organism to a promising active compound is a time-consuming and challenging process which is negatively affecting the overall interest for natural products in drug discovery.[1,2]

Technologies and methodologies have been developed to address these shortcomings.[3] In the early 2000s, implementation of preformatted libraries[4,5] and development of hyphenated techniques[6] and new nuclear magnetic resonance (NMR) probe technologies[7] have accelerated significantly the discovery of bioactive compounds in extracts. This allowed the use of HPLC-SPE-NMR combined with inhibition profiling, for the discovery of bioactive compounds in plant extracts.[8]

More recently, advanced metabolomic tools, such as molecular networking (MN) implemented in global natural product social molecular networking (GNPS),[9] have been established as a drug discovery approach.[10] MN is based on MS fragmentation spectra, which are then linked together on the basis of their similarity. The development of this workflow, driven by a collective effort of academic groups, enables the visualization of features associated with metabolites present in complex extracts and is now used for targeted discovery of natural products.[11] Moreover, significant progress has been made in the structural annotation of such networks.[12] Together with new natural products-oriented chemical classification methods,[13] more advanced approaches allow the classification of unknown metabolites based on their MS fragmentation spectra.[14] Complementing this annotation with confidence scores[15,16] further increases the relevance of such annotations.

By interrogating the molecular network, it is possible to explore the chemical diversity present in an extract and to pinpoint compounds of interest for subsequent isolation. One possibility is to focus on a given biological activity and to look for corresponding features in the data set. Clusters containing features either predicted as biologically active or already reported as active can then be highlighted as potentially interesting, since they most likely include structural analogues

Received: February 11, 2022

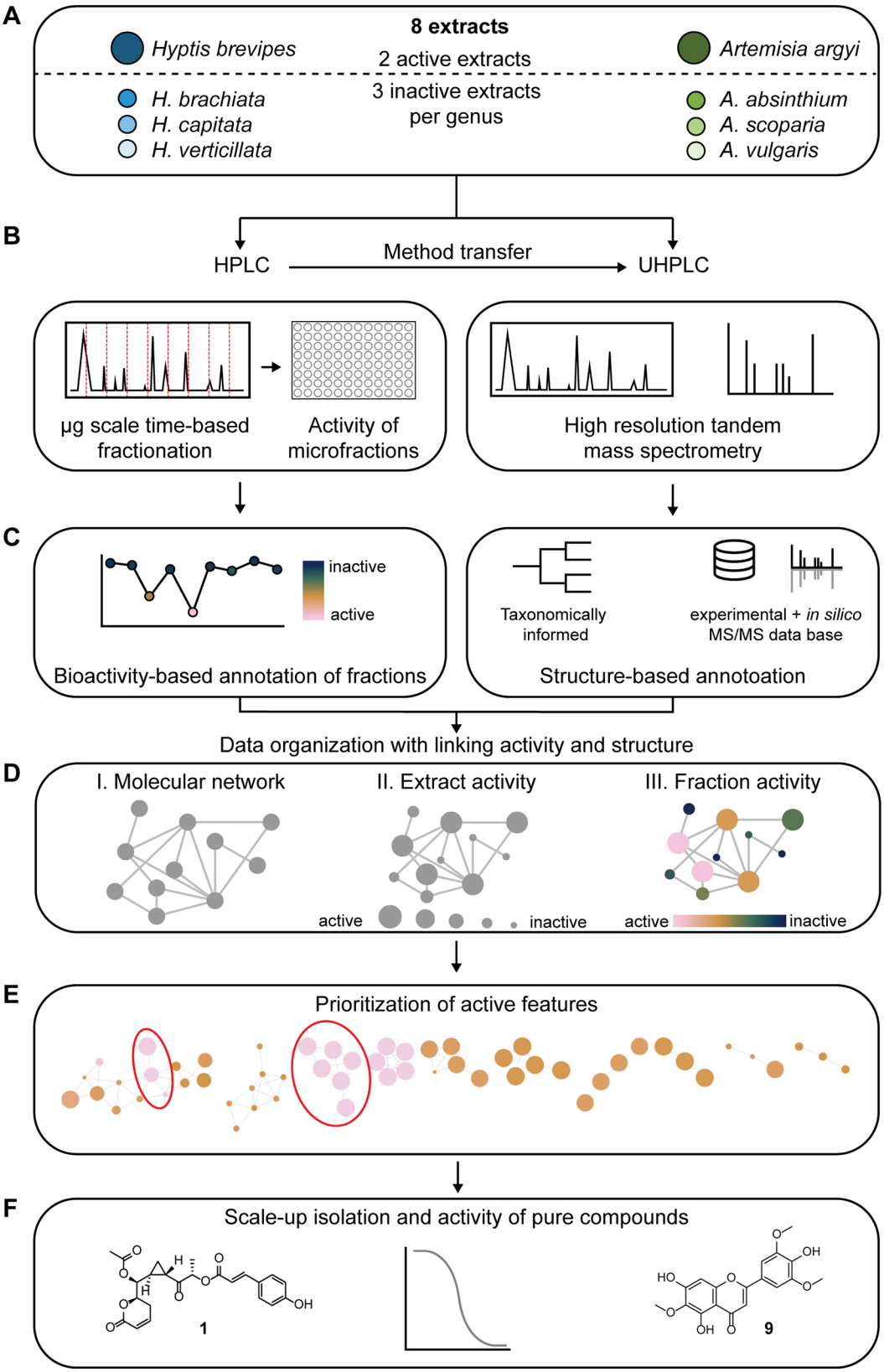

Figure 1. Workflow overview. (A) Eight different plant extracts, including active and inactive extracts from two different genera, were examined. (B) Extracts were submitted to time-based microfractionation by analytical HPLC, and microfractions were submitted to biological testing (left). In parallel, extracts were analyzed by UHPLC-HRMS/MS (right). (C) Activity values obtained were associated with each fraction (left). HRMS/MS data were processed and (structurally) annotated (right). (D) A molecular network was built containing different layers of information, such as structures (I), extract activity associated with the size of nodes (II), and activity of fractions associated with colors of the nodes (III). (E) Features associated with high activity were prioritized and visualized. (F) Selected active features were targeted for isolation, and activity of the isolated compounds was confirmed.

https://doi.org/10.1021/acs.jnatprod.2c00146
J. Nat. Prod. XXXX, XXX, XXX−XXX

that may also be active. This strategy has been used successfully to isolate new analogues of known active compounds.[17,18] While the network can be used to target biologically active compounds, another way to use it is to discover structural novelty.

An extract-based activity annotation was recently reported by Litaudon and co-workers,[19] whereby the MN was based on analytical data and activity of extracts only. In this case, a large data set of closely related extracts (292 extracts from different Euphorbiaceae spp., 20 genera, 107 species) enabled the targeted isolation of specific features on their putative antiviral potential and structural novelty.

A fraction-based activity annotation of the MN has been recently reported. For example, Liang and co-workers developed a workflow where four active extracts from the family Papaveraceae were fractionated on an analytical scale. Fractions were analyzed by LC-CAD-HRMS/MS and tested for biological activities, and a MN was built with this qualitative, semiquantitative, and bioactivity information.[20] A similar approach was used by Dorrestein and co-workers to identify the deoxyphorbol esters responsible for the antiviral activity in an extract of *Euphorbia dendroides*.[21] In this case, the extract was first fractionated on a preparative scale, and each fraction was analyzed and tested. Results obtained from the fractions were added to the network. In these two examples, the MN was built on the basis of data obtained from the fractions and not from the extract. Linking relevant biological activity with features directly in crude extracts would enable an activity-driven approach which, in turn, would significantly accelerate the discovery process.

HPLC-based activity profiling has been used routinely for multiple drug discovery projects since the early 2000s.[22] Depending on the assay type, microgram to submilligram amounts of extract are submitted to a time-based fractionation. The activity of these fractions is then combined with HPLC chromatograms to obtain so-called "HPLC-based activity profiles". Thus, activity can be assigned to discrete fractions/peaks.

To enable the annotation of peaks of interest and to efficiently link these annotated peaks with an activity, the workflow presented herein combines HPLC-based activity profiling with UHPLC-HRMS/MS metabolite annotation to exploit the full potential of both approaches. This resulted in a multilayered MN that was used for the efficient prioritization of two classes of compounds inhibiting AKT activity in human melanoma cells. The prioritized compounds were isolated and tested as active, thus validating the workflow utilized.

RESULTS AND DISCUSSION

Establishment of Workflow for Efficient Prioritization of Active Features. To investigate the combination of HPLC-based activity profiling and advanced UHPLC-HRMS/MS metabolite profiling, eight extracts from a recent plant-based drug discovery project were chosen.[23] Thus, an extract library consisting of over 2500 plant extracts was screened using a scalable high-content screening (HCS) assay that quantifies inhibition of oncogenic ERK (extracellular signal-regulated kinase) and AKT (AK strain transforming kinase) activity in melanoma cells. As outlined in Figure 1A, two active extracts originating from *Artemisia argyi* H. Lév. & Vaniot (Asteraceae) and *Hyptis brevipes* Poit. (Lamiaceae) were selected, together with six inactive extracts from other *Artemisia* and *Hyptis* species. Inclusion of active and inactive extracts of related species is regarded as important in the study design since (1) species belonging to the same genus are more likely to produce similar compounds,[24] (2) specific features responsible for bioactivity should be easier to highlight among species based on comparison of profiling data within the same genus, and (3) annotation confidence is improved by including well-studied species within the genus, with multiple compounds already known. All eight extracts were thus submitted to both HPLC-UV-ELSD activity profiling and UHPLC-HRMS/MS metabolite profiling (Figure 1B,C). The MN obtained on the whole extract data set allowed the organization of the data and to establish links between the extracts and the annotation with different information types, such as dereplicated structures, corresponding natural product classes, the activity of the extracts, and the activity of the microfractions (Figure 1D). In this manner, some clusters of interest were prioritized (Figure 1E) for scale-up isolation, and the activity of the compounds was confirmed subsequently after isolation.

HCS Assay on Melanoma Cells and Activity of Extracts. The HCS assay used throughout this study aimed to identify natural products that target aberrant oncogenic signaling states in melanoma. A patient-derived MM121224 cell line that harbors *BRAF* V600E and *NRAS* Q61K mutations leading to aberrant proliferation through constitutive activation of phosphoinositide 3-kinase/AK strain transforming kinase (PI3K/AKT) and mitogen-activated protein kinase/extracellular signal-regulated kinase (MAPK/ERK) pathway was used.[25] Cells were engineered to express genetically encoded kinase translocation reporters (KTR) that report simultaneously on ERK (ERK-KTR) and AKT (AKT-KTR) activity. In the absence of ERK/AKT activity, the KTR sensors localize to the nucleus of cells, whereas when ERK/AKT activity is high, the KTR sensors get phosphorylated and shuttle to the cytosol in a reversible fashion. Since ERK- and AKT-KTR are labeled with different fluorophores, multiplexed single-cell measurements are possible. The activation status of each kinase can be measured by a ratio of cytosolic versus nucleus fluorescence intensities.[26,27] Finally, an automated image analysis pipeline that enables the analysis of large volumes of images was used to process the data, as described in an earlier paper.[23] This HCS pipeline was used initially to screen 2576 plant extracts.

Eight extracts were selected on the basis of the AKT activity on MM121224 cells obtained from this previous screen and, as described before, included two active and six inactive extracts. These extracts were again submitted for biological testing. The AKT activity is reported as normalized percentage inhibition (NPI), where an NPI $\leq$ 0.4 was considered as strongly active. A NPI between 0.4 and 0.7 was considered as moderately active and values above as inactive. As expected, extracts from *H. brevipes* as well as *A. argyi* exhibited strong inhibition of AKT activity with NPIs of 0.06 and 0.08, respectively. In contrast to the previous screen, extracts from *Hyptis brachiata* Briq. (Lamiaceae) and *Hyptis verticillata* Jacq. (Lamiaceae) showed moderate activity. The other four extracts were inactive (Table S1, Supporting Information). As all extracts were inactive on the ERK pathway (data not shown), in the following workflow only the AKT activity was considered.

HPLC-Based Activity Profiling. Selected extracts were submitted to analytical HPLC-based activity profiling (Figure 1B, left). The amount of extract and HPLC method used to obtain microfractions were adapted to best fit the assay format

https://doi.org/10.1021/acs.jnatprod.2c00146
J. Nat. Prod. XXXX, XXX, XXX−XXX

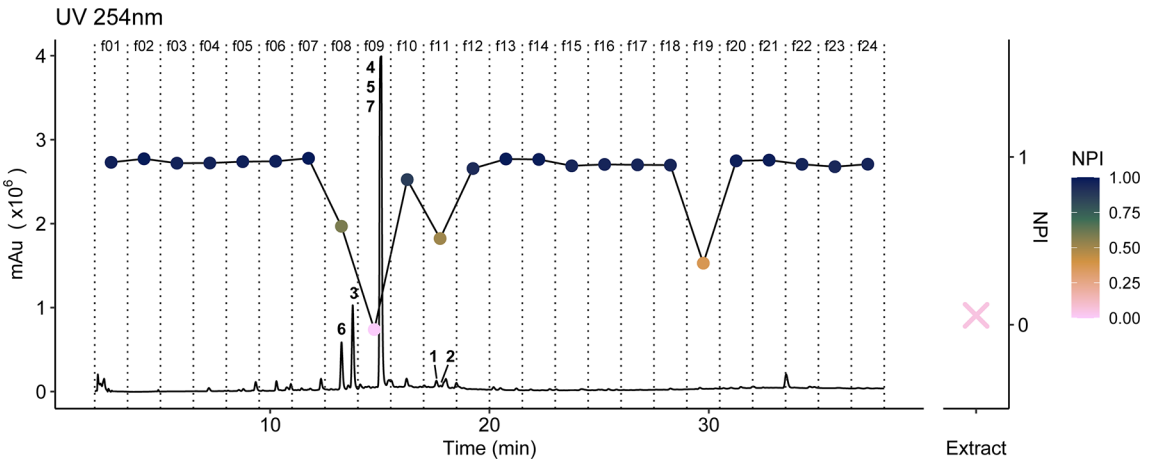

Figure 2. HPLC-based activity profile of the EtOAc extract of *Hyptis brevipes* aerial parts with AKT activity in MM121224 cells. The activity of the crude extract is presented to the right as a cross. The activity of each fraction is represented by a dot; the color scale on the right is used to indicate their activity value, normalized percentage inhibition (NPI). Bold numbers refer to isolated compounds **1**−**7**.

and assay type. In the present work, a submilligram amount of crude extract was fractionated by analytical HPLC in 24 fractions that were tested in the HCS assay. The HPLC-based activity profile of *H. brevipes* extract (Figure 2) indicated four active fractions (activity on AKT in MM121224 cells). Strong and moderate inhibition of AKT activity was also observed in the fractions of *H. brachiata* and *A. argyi* extracts (Figures S2−S5, Supporting Information). However, fractions of *H. verticillata* extract were inactive (Figures S6−S7, Supporting Information). All inactive extracts remained inactive at the fraction level (data not shown). The activity-based information obtained at the fraction level could then be used to annotate the MN (Figure 1D III).

HPLC-UHPLC-MS/MS Geometrical Chromatographic Gradient Transfer. In order to link the "HPLC-based bioactivity data" with "UHPLC metabolite profiling data" both chromatographic methods had to be precisely correlated. For this, the HPLC conditions were optimized to ideally fit the activity testing purposes and were taken as the starting point for the geometrical chromatographic gradient transfer to UHPLC (Figure 1B), as described by Guillarme et al.[28] HPLC and UHPLC stationary phases were the same to ensure ideal transfer. To avoid small inaccuracies, particularly at the beginning of the gradient, retention times were normalized between the first and last observed peaks. This resulted in HPLC fraction times transferable to the UHPLC conditions, thus avoiding a systematic analysis of all fractions on the UHPLC platform. An example of such transferred retention time windows is shown in Figure S6 and S7 (Supporting Information). After this was done, the activity of the fractions was mapped on the corresponding normalized retention time window of the UHPLC run.

UHPLC-MS/MS Data Organization and Usage for Prioritization. The UHPLC-PDA-CAD-HRMS/MS data was treated with MZmine using the recently introduced ion identity.[29] It was then processed through the GNPS to lead to a hybrid MN containing both MS1 and MS2 information to organize the data.

The network obtained is shown in Figure 3A. Clustering parameters were adapted to maintain maximum connectivity between nodes, thus maximizing information. Further details can be found in the related Experimental Section. Features were, in parallel, annotated with taxonomic, structural, and bioactivity information. The annotation of the features with biological information was made through the calculated retention time window. All features were informed with a refined NPI value, as described in the Experimental Section, allowing a more precise selection of features to prioritize. Features annotated with an NPI value <0.7 were considered as active and were prioritized. Edges to nonactive features were discarded (Figure 3B), and the MN was reorganized according to remaining edges (Figure 3C). The advanced annotation of the MN is illustrated in Figure 3D. As all analytical runs were acquired in the same batch, the source organism(s) of the feature could be attributed to those in the extract where the three most intense signals were found.

The entire processing and data organization were performed to rationally reduce features/data dimension to a meaningful subset that allows expert evaluations for prioritization. Out of 214 features that were linked to an interesting NPI value (≤0.4), 80 belonged to clusters with at least four features (Figure 3C). These clusters were annotated mainly as brevipolides, flavonoids, triterpenoids, diterpenoids, and sesquiterpenoids (mainly sesquiterpene lactones).

The two larger clusters, clusters 1 and 2, were analyzed and annotated in more depth (Figure 4). Cluster 1 did contain features belonging to mainly one extract, and these features were annotated as being very active (highlighted in pink). On the other hand, cluster 2 displayed features from different extracts, suggesting the presence of less taxon-specific compounds associated with an activity. Best-candidate structures coming from the GNPS and ISDB-LOTUS[30,31] complemented with pairs coming from the *Dictionary of Natural Products* are reported. Details concerning the candidate taxonomically informed weighting, are provided in the Experimental Section.

In cluster 1, features were present almost exclusively in *H. brevipes*. Their activity scores were the highest among all features, and they could be annotated as brevipolides, described earlier from *H. brevipes*.[32−34] Interestingly, a diterpenoid with abietane skeleton reported previously from *H. dilatata*[35] was also annotated in the middle of the brevipolide cluster. In total, with stereoisomers, four of the annotated structures in cluster 1 were confirmed by later isolation (see related section).

https://doi.org/10.1021/acs.jnatprod.2c00146
J. Nat. Prod. XXXX, XXX, XXX−XXX

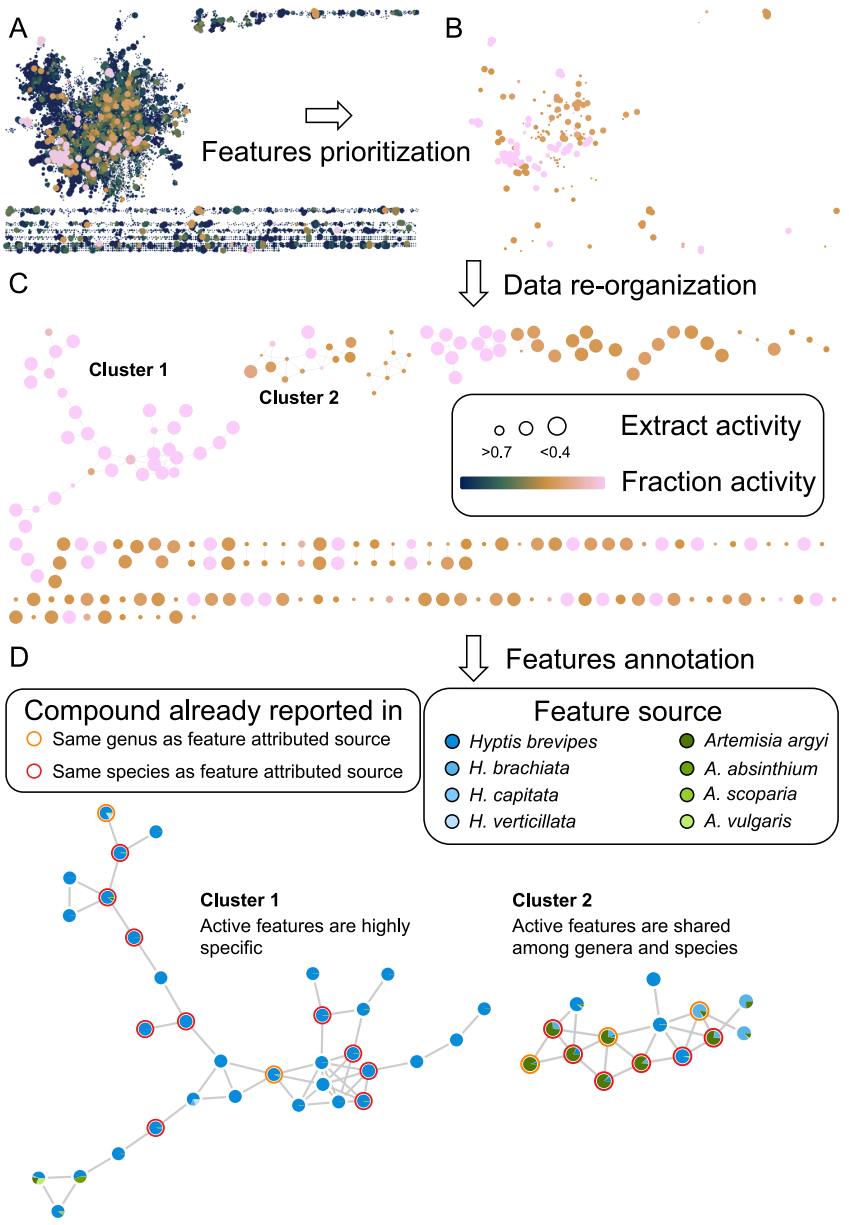

Figure 3. Overview of the Molecular Network (MN). (A) The obtained MN, without self-loops. (B) The nodes considered as active are prioritized. Nodes are highlighted according to color scale (pink for NPI = 0.0; beige for NPI = 0.4, green for NPI = 0.7 and blue for NPI = 1.0) and edges to nonactive features removed. (C) The data are reorganized according to the remaining edges. (D) The two most interesting clusters after metadata addition.

In cluster 2, nodes with the highest activity score again were found mainly in *H. brevipes*, but some other related nodes also exhibiting reasonable activity occurred in *A. argyi* and *H. brachiata*. All annotated nodes were methoxylated flavonoids, with the exception of an anthraquinone derivative coming from the GNPS library (CCMSLIB00006422349). Based on the structure, it was possible to see the structural moiety of the anthraquinone leading to similar fragments as the methoxylated flavonoids to explain this inconsistency. Among the methoxylated flavonoids cluster, only one structure was annotated correctly. The difficulty of correct identification lay in determining the exact positions of the methoxylated group of these flavonoids, which do not lead to significant differences in the corresponding fragmentation spectra. As an example, 6-methoxytricin (**9**), isolated in this work, was annotated as an isomer that had only one small modification among its substituents. Compound **9** has one methoxy moiety at C-3′ and one hydroxy group at C-4′. However, the position of these substituents was inverted in the annotated feature. Some of the annotated methoxylated flavonoids were already reported either in *H. brevipes*,[32] *A. argyi*,[36−41] or related *Artemisia* species.[42]

Annotations were highly consistent within both the brevipolide and methoxylated flavonoid molecular families, and so isolation efforts were focused on those active labeled features. Tabulations detailing prioritized features are available in Tables S2 and S3 (Supporting Information), together with related extracted ion chromatograms (Figures S16−S18, Supporting Information).

Scale-up Isolation of Prioritized Compounds. Brevipolides as well as some flavonoids highlighted in the prioritization workflow were identified from a large-scale

https://doi.org/10.1021/acs.jnatprod.2c00146
J. Nat. Prod. XXXX, XXX, XXX−XXX

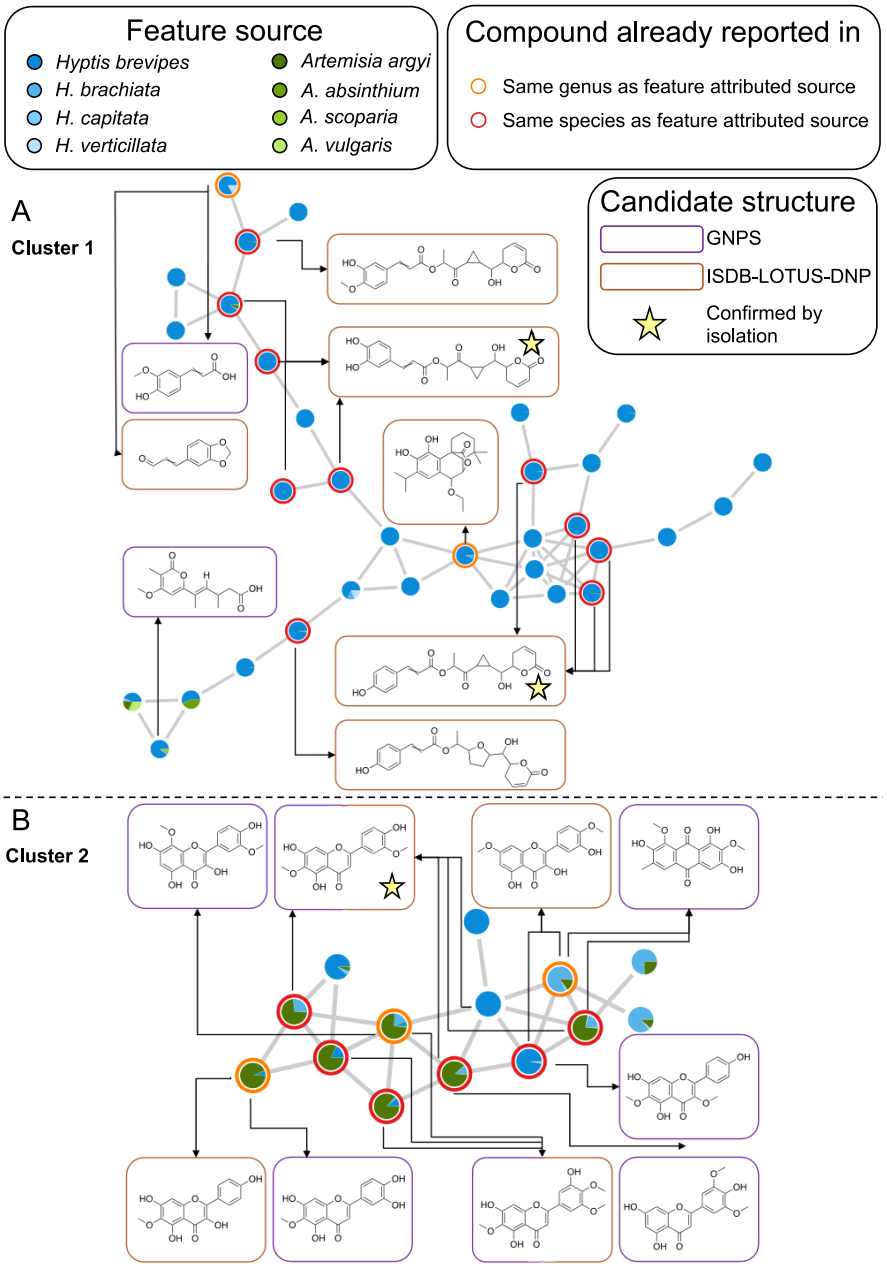

Figure 4. Two most interesting clusters. (A) Cluster 1, containing highly specific features of *Hyptis brevipes* extract annotated as brevipolides. (B) Cluster 2, containing features shared among different extracts and annotated as methoxylated flavonoids.

EtOAc extract of *H. brevipes* and isolated as compounds **1**–**7**. Their planar structures were elucidated by NMR spectroscopy and identified on the basis of comparison with literature values as brevipolide A (**1**),[32] brevipolide B (**2**),[32] brevipolide C (**3**),[32] brevipolide F (**4**),[32] brevipolide G (**5**),[33,43] 3,7-dimethylquercetagetin (**6**),[44] and chrysosplenol C (**7**).[45] The isolated brevipolides (**1**–**5**) have been previously reported in *H. brevipes*,[32,33] but, to the best of our knowledge, the two flavonoids **6** and **7** are new to the genus *Hyptis*.

Additional methoxylated flavonoids were annotated in *H. brachiata* and *A. argyi*. A scale-up extract of *H. brachiata* afforded sideritoflavone (**8**),[46] which already has been reported from other *Hyptis* species.[47−49]

One fraction, namely, fraction N, obtained in a previous investigation on *A. argyi*,[50] was determined as containing mainly flavonoids. Further purification of this fraction led to the isolation of compounds **9**–**12**. These were identified as 6-methoxytricin (**9**), jaceosidin (**10**), eupatilin (**11**), and chrysosplenetin (**12**). All compounds are known as constituents of *A. argyi*, except for 6-methoxytricin, which was so far reported only in other *Artemisia* species (Chart 1).[51−54]

Absolute Configurations of Brevipolides. The absolute configuration (AC) for brevipolides A–G was established previously as 5*R*, 6*S*, 7*S*, 9*S* using a combination of NOESY, ECD, and Mosher's method, without being able to resolve the AC at C-11.[32] This was later established as 11*S* by X-ray crystallography and hydrogenation for brevipolides H and I. The AC of all other brevipolides was suggested to be the same at C-11 considering similarity in experimental and theoretical NMR and ECD data.[33] However, the calculated spectra of both C-11 epimers had not been studied. We, therefore, compared the experimental ECD spectra to ab initio calculated

https://doi.org/10.1021/acs.jnatprod.2c00146
J. Nat. Prod. XXXX, XXX, XXX−XXX

Chart 1. Compounds Isolated from *Hyptis brevipes* (1–7), *Hyptis brachiata* (8), and *Artemisia argyi* (9–12) Extracts

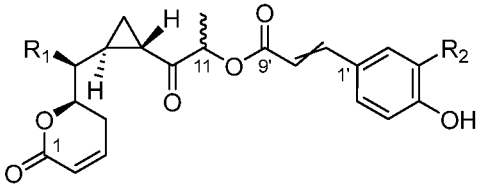

	R_1	R_2	
1	OCH_3	H	(*trans*) 11*R*
2	OCH_3	H	(*cis*)
3	OH	OH	(*trans*) 11*R*
4	OH	H	(*cis*)
5	OH	H	(*trans*) 11*R*

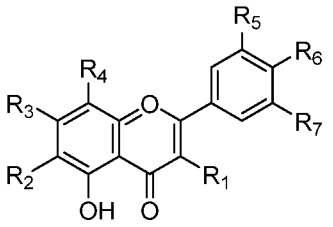

	R_1	R_2	R_3	R_4	R_5	R_6	R_7
6	OCH_3	OH	OCH_3	H	OH	OH	H
7	OCH_3	OH	OCH_3	H	OCH_3	OH	H
8	H	OCH_3	OCH_3	OCH_3	OH	OH	H
9	H	OCH_3	OH	H	OCH_3	OH	OCH_3
10	H	OCH_3	OH	H	OCH_3	OH	H
11	H	OCH_3	OH	H	OCH_3	OCH_3	H
12	OCH_3	OCH_3	OCH_3	H	OCH_3	OH	H

reference spectra of both epimers at C-11 to assign the configurations.

The main difference between the experimental spectra of *trans*- and *cis*-brevipolides in their ECD was the sign of the band around 300 nm (representative examples are shown in Figure 5) as described earlier.[33] In addition, experimental ECDs of both *trans*- and *cis*-brevipolides show a negative Cotton effect (CE) around 228 nm and a positive CE at 260 nm.

The ECD spectra of both C-11 epimers of *trans*- and *cis*-brevipolides were calculated (Figures 5 and S20, S22, S24, Supporting Information). In all *trans*-brevipolides, the calculated spectra of the 11*S*-epimers typically showed negative CEs at 228 nm and positive CEs at 260 nm. Moreover, the spectra displayed a positive or no significant CE at 300 nm (Figures 5A and S20, S24, Supporting Information). In contrast, the calculated spectra of all 11*R*-epimers did exhibit a positive CE at 260, no negative CE at 228 nm, and in brevipolides A and G an additional positive CE at 275 nm. Moreover, they showed a distinct negative CE around 300 nm. As the calculated CE at 300 nm was very distinct for both C-11 epimers, the assignment of the 11*S*-configuration could be defined clearly for the *trans*-brevipolides A (**1**), C (**3**), and G (**5**).

For the two *cis*-brevipolides, no clear conclusion could be reached, as the differences between the calculated spectra were much less pronounced or virtually nonexistent (Figures 5B and S22, Supporting Information). A reason could be the negative CE at 300 nm, which was previously described as typical for *cis*-brevipolides, and coincides with the negative CE around 300 nm calculated for all 11*R* epimers.[33] Thus, ECD was not suited to assign the ACs at C-11 for *cis*-brevipolides B (**2**) and F (**4**). However, as all ^{13}C NMR shifts for C-11 are very similar, this suggests a common *S*-configuration at this position for all compounds.

Activity of Isolated Compounds. While only AKT activity readouts were considered for MN analysis, the results of both ERK and AKT activity in response to the isolated compounds were determined.

All brevipolides exhibited a strong concentration-dependent inhibition of AKT activity, whereas the ERK activity was, as expected, less affected (Figure 6, and S25, Supporting Information). However, at the highest concentration of 200

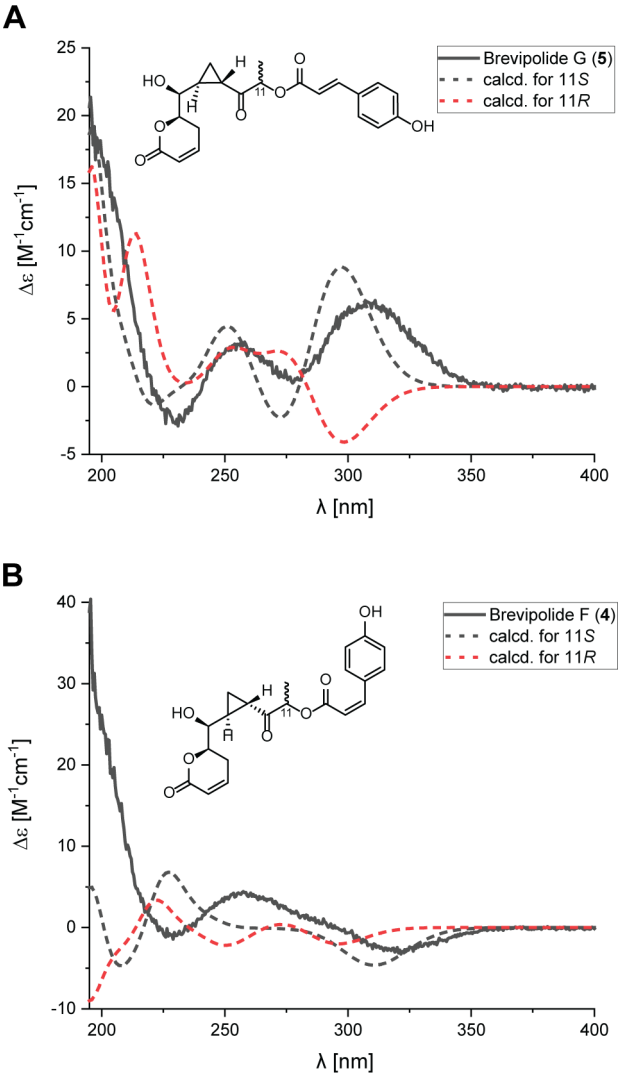

Figure 5. ECD spectra of brevipolide G (**5**) and brevipolide F (**4**). Experimental ECD spectra (black line) are compared to the calculated ECD spectra of the 11*S*- and 11*R*-epimers (dashed lines) in MeOH (calculated spectra shifted by +10 nm).

https://doi.org/10.1021/acs.jnatprod.2c00146
J. Nat. Prod. XXXX, XXX, XXX−XXX

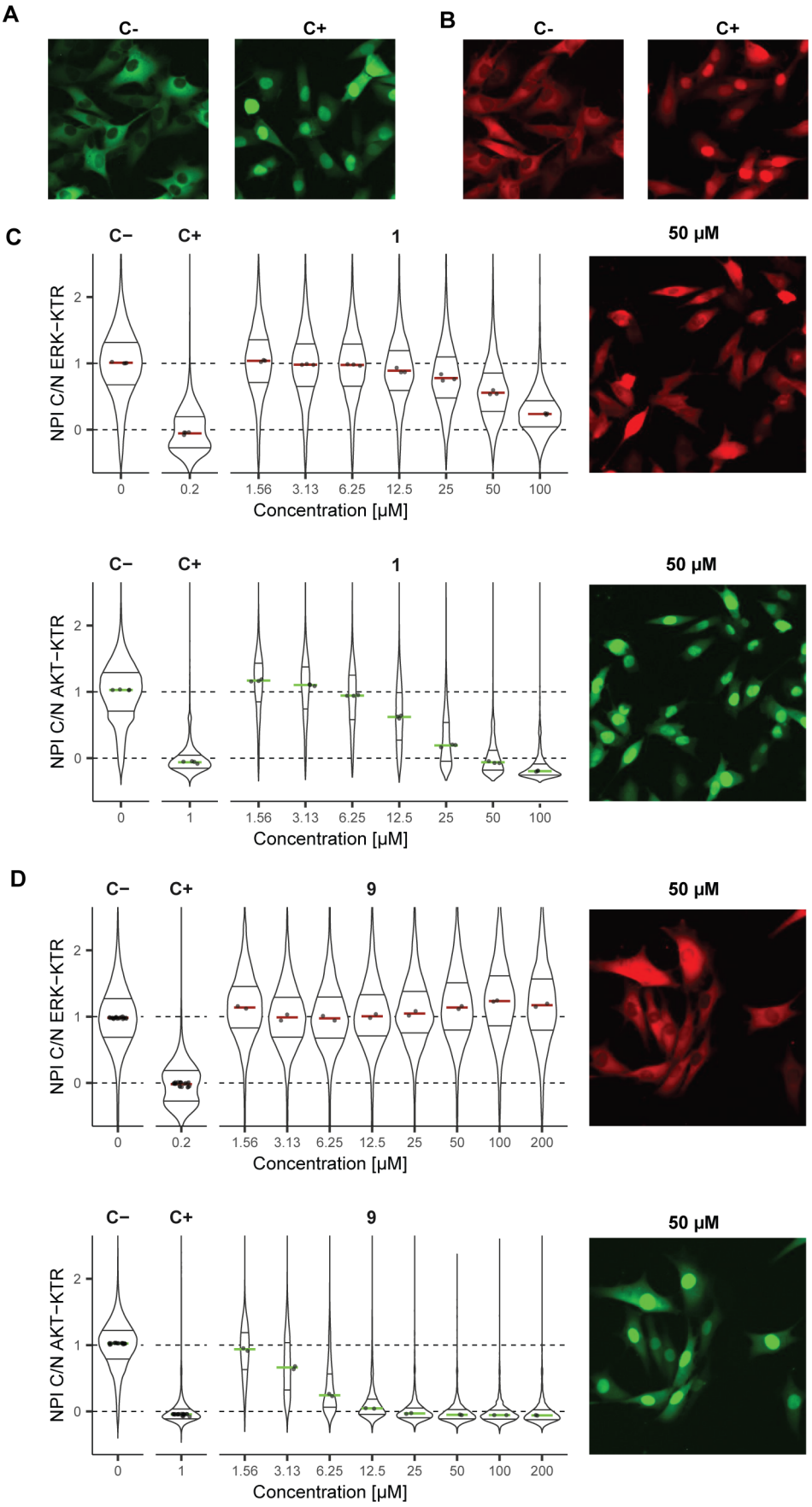

Figure 6. Representative images of positive and negative controls of the AKT-KTR (A) and ERK-KTR (B) in MM121224 cells. Concentration response curve for brevipolide A (**1**) (C) and 6-methoxytricin (**9**) (D) on ERK and AKT activity in MM12224 with representative images. C+ and

https://doi.org/10.1021/acs.jnatprod.2c00146
J. Nat. Prod. XXXX, XXX, XXX−XXX

Figure 6. continued

C- designate positive (1 μM GDC0941 as PI3K/AKT pathway inhibitor, 200 nM cobimetinib as MAPK/ERK pathway inhibitor) and negative (0.75% DMSO) controls. Data distribution from single MM121224 cells are represented as a violin plot; the median of treatment distribution (middle bar), as well as the first and third quartiles, are shown. Data are taken from at least 200 cells. The brightness of representative images was adapted per 96-well plates.

μM (100 μM for brevipolide A, **1**), lower cell numbers, as well as rounding up of the cells were observed, indicating cell toxicity. Among these compounds, brevipolide A (**1**) was the most potent with a relative IC_{50} of 17.6 ± 1.6 μM on AKT (Figure 6). The IC_{50} values for **2**−**5** were determined as 32.9 ± 3.4, 61.7 ± 9.6, 53.5 ± 9.9, and 32.3 ± 5.6 μM against AKT, respectively. There were no IC_{50} values determined for ERK in the MM121224 cells used, because no plateau was reached at 200 μM (respectively, 100 μM).

Brevipolides A (**1**), B (**2**), F (**4**), and G (**5**) were reported previously to be cytotoxic against different cancer cells. Brevipolide C (**3**) is known to inhibit the proteasome, while brevipolide G reportedly inhibits NF-κB.[32] An updated study of brevipolide pharmacology was published recently, in which brevipolide H was examined. With a methoxy group instead of a hydroxy group at C-4′, brevipolide H is closely related to brevipolide G. In this report, brevipolide H was shown to reduce AKT activity using Western-blot experiments.[55] The inhibitory activity of brevipolides A−C, F, G (**1**−**5**) on AKT signaling support these earlier findings on brevipolide H.

The most active flavonoid **9** had an IC_{50} value of 4.9 ± 0.2 μM, whereas compounds **8**, **10**, **11** were also active at a low μM range (27.9 ± 2.8, 11.1 ± 1.1, and 20.9 ± 2.7 μM, respectively) (Figures 6, S28, and S29, Supporting Information). For the less active compounds **6**, **7**, and **12**, which all bear a methoxy group at C-3, a 100% inhibition was not reached (Figure S28 and S29, Supporting Information). Within the series of methoxylated flavonoids, it was the first time that compounds **8** and **9** were identified as downregulating AKT activity in melanoma. Previous studies have suggested that eupatilin (**11**) specifically inhibits PI3K kinase,[56] and phosphorylated AKT was shown to be decreased in jaceosidin treated cells.[57] The general potential of flavonoids in inhibiting the phosphorylation of AKT was studied in a screen of 44 phenolic compounds, where 26 compounds showed activity via ELISA and Western blot experiments.[58] Furthermore, it is interesting to mention that a morpholine-containing small molecule, compound LY294002, developed as an ATP competitive inhibitor of PI3K enzymes, was derived from the basic structure of a flavonoid (quercetin).[59] These examples highlight the potential of flavonoids as PI3K/AKT inhibitors.

CONCLUSION

The main goal of the current work was to investigate how HPLC-based activity profiling can be rationally combined with advanced UHPLC-HRMS/MS metabolite profiling. The workflow developed here allowed data organization and annotation to efficiently link activity with compounds contained in crude extracts, thereby facilitating the prioritization of features for scale-up isolation of active natural products. The tagging of bioactive features present in crude extracts was confirmed by the isolation of two classes of compounds that were subsequently tested as active.

The miniaturization and scalability of the HCS platform provided the necessary throughput to efficiently characterize the antioncogenic ERK/AKT activity of a range of compound analogues. Thus, brevipolides A−C, F, G (**1**−**5**) were all shown to downregulate AKT, a finding that is in line with results obtained with Western blot on the related brevipolide H.[55] This example highlights the advantages of HCS assays in the context of library screening and rapid characterization of compound series.

By combining activity profiling with advanced annotation, information obtained by each of the approaches could be leveraged. On the one side, the activity-profiling approach provides activity data at the microfraction level, thereby improving the quality of the annotation. In comparison to an extract-based activity annotation, the number of features being active is significantly reduced. This advanced annotation even allowed the identification of an active methoxylated flavonoid from *H. brachiata* which would not have been identified as active by using the activity profiling approach alone.

Nevertheless, some of the limitations inherent to each approach will remain. Activity profiling will still be affected, for example, by peaks eluting in two adjacent fractions. Moreover, feature annotation could be biased by the over-representation of compound classes already well described, both structurally and for their activity.[60]

Since metabolite and activity profiling both allow for high throughput, lowering it to medium throughput appears as a good compromise between speed and data quality. Longer LC gradient times, for example, allow for better discrimination of isomers, better peak shapes, and more accurate gradient transfer. This also affords more fractions for bioactivity testing, allowing better localization of the activity within an extract. While slightly increasing experimental time, this undoubtedly leads to better prioritization of active features, and later validation of the predicted active features.

Finally, while the presented results were obtained in a screen for natural products inhibiting oncogenic signaling in melanoma, the developed methodology can be used with any modern bioassay pipelines that allow for both miniaturization and scalability. It is expected also that this workflow will be useful when trying to better understand an observed activity resulting from a complex extract. This is of great importance for natural products drug discovery, as highlighted here, and also of great potential for the identification of active principles in phytomedicines, and for the rapidly growing fields of nutraceuticals and cosmetics containing plant derived compounds.

EXPERIMENTAL SECTION

General Experimental Procedures. UV and ECD spectra were recorded in MeOH (66.6−133.3 μg/mL) on a Chirascan CD spectrometer using 1 mm-path precision cells (110 QS, Hellma Analytics, Müllheim, Germany). NMR spectra were recorded on a Bruker Avance III NMR spectrometer operating at 500.13 MHz for ^{1}H and 125.77 MHz for ^{13}C nuclei. ^{1}H NMR, COSY, HSQC, HMBC, and NOESY spectra were measured at 23 °C in a 1 mm TXI or a 5 mm BBO probe. Spectra were recorded in $CDCl_3$ (Sigma-Aldrich, St. Louis, MO, U.S.A.), acetone-*d*, or DMSO-d_6 (both Armar Chemicals, Döttingen, Switzerland). Bruker TopSpin 3.5 and ACD/Laboratories NMR Workbook suites softwares were used to process the data.

https://doi.org/10.1021/acs.jnatprod.2c00146
J. Nat. Prod. XXXX, XXX, XXX−XXX

Chemical shifts are reported as δ values (ppm), with residual signal as internal reference, J in Hz.

HPLC-grade solvents MeOH, CH_3CN (Avantor, Radnor, PA, U.S.A.) and water from a Milli-Q water purification system (Merck Millipore, Billerica, U.S.A.) were used for HPLC separation. HPLC-grade formic acid (FA) and DMSO were obtained from Scharlau (Scharlab S.L., Spain). For extraction and silica gel column chromatography, technical-grade *n*-hexane, EtOAc, and MeOH and HPLC-grade $CHCl_3$ were used (Rheuss Chemie, Tägerig, Switzerland). Normal-phase flash chromatography was carried out on a Puriflash 4100 system (Interchim, Montluçon, France) consisting of a pump, a UV detector and fraction collector. Silica gel 60 (15−40 μm to pack column; 63−200 μm for dry loading) was obtained from Merck. TLC analysis was performed on silica gel 60 F_{254} coated aluminum TLC plates (Merck, Darmstadt, Germany). Detection occurred at UV 254 and 366 nm, and after spraying with 1% ethanolic vanillin and 10% sulfuric acid in EtOH, followed by heating (10 min; 110 °C). Preparative HPLC separation was carried out on a 1290 Infinity II Preparative LC/MS system (Agilent Technologies, Santa Clara, CA, U.S.A.) consisting of a binary pump connected to a PDA and to a single quadrupole MS detector via a T-splitter. A SunFire Prep C_{18} OBD column (5 μm, 30 × 150 mm i.d., Waters, Milford, MA, U.S.A.) equipped with a C_{18} Prep guard column (10 × 30 mm i.d.) was used. The flow rate was 20 mL/min. Semipreparative HPLC was carried out on a HP 1100 Series system (Agilent Technologies, Santa Clara, U.S.A.) consisting of a binary pump, an autosampler, and a DAD or on an Alliance HPLC system 2690 (Waters, Milford, MA, U.S.A.) equipped with a DAD 996 detector (Waters). Separations were carried out at a flow rate of 4 mL/min. The following semiseparative RP-HPLC columns were used: SunFire Prep C_{18} column (5 μm, 10 × 150 mm i.d., Waters, Milford, MA, U.S.A.) equipped with a guard column (10 × 10 mm i.d.) for *H. brevipes* and *A. argyi* and a ReproSil-Pur 120 C_{18}-AQ column (3 μm, 10 × 150 mm i.d., Dr. Maisch GmbH, Ammerbuch-Entringen, Germany) and for *H. brachiata*.

Microfractionation and analytical HPLC-PDA-ELSD-ESIMS (for activity profiles) were carried out on a LC-MS 8030 system (Shimadzu, Kyoto, Japan) consisting of degasser, binary high-pressure mixing pump, autosampler, column oven, and PDA detector. A triple quadrupole MS and an ELSD 3300 detector (Alltech, Deerfield, IL, U.S.A.) were connected via a T-splitter to the system. The mobile phases contained 0.1% FA. An XBridge C_{18} (3.5 μm, 3.0 × 150 mm i.d.) column equipped with a VanGuard precolumn (3.5 μm, 2.1 mm × 5 mm i.d.) (both Waters, Milford, MA, U.S.A.) was used.

UHPLC analysis was performed on a Waters Acquity UPLC system (Waters, Milford, MA, U.S.A.) with photodiode array (PDA) (Waters) interfaced to a Q-Exactive Focus mass spectrometer (Thermo Scientific, Bremen, Germany) and a Charged Aerosol Detector (CAD) (Thermo Scientific, Bremen, Germany) using a heated electrospray ionization (HESI-II) source. Thermo Scientific Xcalibur 3.1 software with SII and specific drivers for CAD were used for instrument control. The mass analyzer was calibrated using a mixture of caffeine, methionine−arginine−phenylalanine−alanine−acetate (MRFA), sodium dodecyl sulfate, sodium taurocholate, and Ultramark 1621 in a $CH_3CN/MeOH/H_2O$ solution containing 1% FA by direct injection. The data-dependent MS/MS events were performed on the three most intense ions detected in full-scan MS (Top3 experiment). The MS/MS isolation window width was 1.5 Da, and the stepped normalized collision energy (NCE) was set to 15, 30, and 45 units. In data-dependent MS/MS experiments, full scans were acquired at a resolution of 35,000 fwhm (at m/z 200) and MS/MS scans at 17,500 fwhm both with a maximum injection time of 119 ms and 55 ms, respectively. After being acquired in a MS/MS scan, parent ions were placed in a dynamic exclusion list for 2.0 s. Diisooctyl phthalate $C_{24}H_{38}O_4$ $[M + H]^+$ ion (m/z 391.28429) was used as an internal lock mass. The optimized HESI-II parameters for the long runs were as follows: source voltage, 3.5 kV (positive); sheath gas flow rate (N_2), 38 units; auxiliary gas flow rate, 10 units; auxiliary gas temperature, 266 °C; sweep gas flow rate, 1 unit; capillary temperature, 250 °C; S-Lens RF Level, 45. For short runs: source voltage, 3.5 kV (positive); sheath gas flow rate (N_2), 45 units; auxiliary gas flow rate, 10 units; auxiliary gas temperature, 400 °C; sweep gas flow rate, 2 units; capillary temperature, 250 °C; S-Lens RF Level, 45. Separation was achieved on an Acquity BEH C_{18} column (2.1 × 50 mm I.D.; 1.7 μm) (Waters) for the short runs, and on an Acquity BEH C_{18} column (2.1 × 150 mm I.D.; 1.7 μm) (Waters), both equipped with a precolumn of 5 mm of the same phase. The temperature in the autosampler and column oven was fixed at 10 and 40 °C, respectively. The mobile phase consisted of water (A) and CH_3CN (B) both containing 0.1% FA; separation was performed with a linear gradient from 5 to 100% of B in 3.42 min with an initial hold of 0.17 min at 5% followed by a 1 min isocratic step at 100% of B and then a 1 min isocratic step at 5% of B for column reconditioning. For long runs, separation was performed with a linear gradient from 5 to 100% of B in 59.00 min with an initial hold of 1.18 min at 5% followed by a 17 min isocratic step at 100% of B and then an 11 min isocratic step at 5% of B for column reconditioning. The injection volume was set at 2 μL for both runs, and the flow rates were fixed at 0.6 mL/min and 0.4 mL/min, respectively. A PDA was used to acquire UV spectra detected from 200 to 500 nm. The CAD evaporation temperature was set at 40 °C, with 5 bar N_2, and power function 1, and a data collection rate of 20 Hz with a 0.5 s filter constant. The analytical flow splitter was an ASI 610 Series and was set to 62, which corresponded to a 2:1 ratio (CAD:MS).

Plant Material. *Hyptis brevipes* aerial parts were collected in San Antonio (Panama) in November 1990, by the Centro de Investigaciones Farmacognosticas de la Flora Panamena (CIFLORPAN). *Hyptis brachiata* aerial parts were collected in the area of El Pinar, Coclé Province (Panama) by CIFLORPAN. The taxonomic identity of *H. brevipes* and *H. brachiata* was confirmed by Alex Espinosa, a botanist at CIFLORPAN, and voucher specimens are deposited at the Herbarium of the University of Panama (*H. brevipes* ground plant material, no. 1183; *H. brachiata*, no. 391). The material was dried and ground in Panama. Voucher specimens are also available at the Division of Pharmaceutical Biology, Department of Pharmaceutical Sciences, University of Basel (no. 1183; 1181). *Artemisia argyi* whole plant material was purchased from Peter Weinfurth, Bochum, Germany, in March 2016 (batch no. 150788859). A voucher specimen (no. 00 979) is deposited at the Division of Pharmaceutical Biology, University of Basel, Switzerland.

Microfractionation and Activity Profiles. The following EtOAc extracts (10 mg/mL in DMSO) from an in-house library were microfractionated and tested: *H. brachiata* (Lamiaceae), *H. brevipes* (Lamiaceae), *Hyptis capitata* Jacq. (Lamiaceae), *H. verticillata* (syn. *Condea verticillata* (Jacq.) Harley & J.F.B. Pastore) (Lamiaceae), *Artemisia absinthium* L. (Asteraceae), *A. argyi* (Asteraceae), *Artemisia scoparia* Waldst. & Kit. (Asteraceae), and *Artemisia vulgaris* L. (Asteraceae).

Microfractionation of the extracts was carried out on an LC-MS 8030 system (Shimadzu, Kyoto, Japan) connected to an FC 204 fraction collector (Gilson, Middleton, WI, U.S.A.) adapted for 96-deep-well plates. Three injections of each extract were carried out: 2 × 30 μL (corresponding to 600 μg of extract) using only the PDA detector for collection of microfractions, and 1 × 10 μL with PDA-ELSD-ESIMS detection without collection. Water with 0.1% FA (A) and CH_3CN with 0.1% FA (B) were used as mobile phases. The gradient started with an initial 10% B for 2 min, followed by a gradient to 100% B in 28 min, and a final hold at 100% B. Fractions of 1.5 min each were collected from min 2 to min 38, resulting in 24 fractions. The microfractions of the two successive runs were collected into the same well of a 96-deep-well plate. The plate was dried in a Genevac EZ-2 evaporator. The HPLC-ELSD or HPLC-UV chromatogram was combined with the activity of fractions to generate the so-called activity profile.

UHPLC-MS/MS Data Analysis Pipeline. After conversion to the.mzML format with ThermoRawFileParser[61] to also encode the CAD signal, a custom version of MZmine (https://github.com/robinschmid/mzmine2/releases) was used to perform the Ion Identity UHPLC-HRMS/MS data processing.[29]

https://doi.org/10.1021/acs.jnatprod.2c00146
J. Nat. Prod. XXXX, XXX, XXX−XXX

During the mass detection step, the ions kept were those above a noise level set at 1.0E5 for MS1 (and 0 for MS2). Chromatogram builder was employed with a minimum height of 1.0E5 and m/z tolerance of 0.02 Da. The chromatogram deconvolution was performed using the wavelets ADAP algorithm[62] with a single noise (S/N) threshold of 3.3, the wavelet scales from 0.00 to 0.10 min, and a peak duration range from 0.02 to 3.00 min; the MS2 scan pairing was set at m/z 0.02 Da (0.2 min). The chromatograms were deisotoped using the isotope peak grouper with an m/z tolerance of 10 ppm, a retention time (RT) tolerance of 0.1 min, and a maximum charge of 3, while the representative isotope used was the most intense. Peak alignment was applied using the join aligner method with an m/z tolerance of 10 ppm, an RT absolute tolerance at 0.1 min, and weight for m/z and RT of 1. The peak list was gap-filled using the multithreaded peak finder module with a peak shape tolerance of 100%, an m/z tolerance of 10 ppm, and 0.1 min. Duplicated features were removed. Manual curation was performed on the peak list. Additionally, features were filtered between 0.5 and 77.5 min and with a peak duration range between 0.02 and 3.00 min. Feature IDs were reset. An ion identity module was used with 10 ppm tolerance, a minimum height of 1E5, and a minimum cluster size of 2. Networks without major monomers were discarded. Multiple steps of adducts and modifications annotations were performed, including custom lists. Finally, ion identities were checked by MS/MS, with an MS2 tolerance of 10 ppm and a minimal MS2 height of 50. Multimers and neutral losses were checked. Once done, a custom script was built to remove the gap-filled area and reintegrate the features using the gap-filling module again with a peak shape tolerance of 0%, an m/z tolerance of 10 ppm, and 0.1 min. Data were exported using both GNPS and SIRIUS export modules, allowing to merge MS/MS spectra across samples by a weighted average, summing their intensities, with an expected mass deviation of 10 ppm, a cosine threshold of 65%, a peak count threshold of 20%, no isolation window offset, and an isolation window width of 3 Da. To keep the retention time, the exact mass information and to allow for the separation of isomers, an ion identity molecular network was created using the export resulting from the MZmine pretreatment step detailed above.

A network was then created on GNPS[9] where edges were filtered to have a cosine score above 0.6 and more than six matched peaks. Further edges between two nodes were kept in the network if and only if each of the nodes appeared in the respective top 20 most similar nodes of one anohter. The spectra in the network were then searched against the GNPS spectral libraries. The precursor ion mass tolerance was set to 0.02 Da and the MS/MS fragment ion tolerance to 0.02 Da. A MN was then created where edges were filtered to have a cosine score above 0.6 and more than 6 matched peaks. Further, edges between two nodes were kept in the network only if each of the nodes appeared in each other's respective top 20 most similar nodes. Finally, the maximum size of a molecular family was set to 0, and the lowest-scoring edges were removed from molecular families until the molecular family size was below this threshold. The spectra in the network were then searched against the GNPS spectral libraries.[9,63] All matches kept between network spectra and library spectra were required to have a score above 0.6 and at least six matched peaks. Additional edges coming from IIN processing were added. The GNPS job parameters and resulting data are available at the following address (https://gnps.ucsd.edu/ProteoSAFe/status.jsp?task=828243dd50da4fd2ad94d25ba5e559c9). The full MS data set is uploaded and accessible on the GNPS servers as Massive Data sets N° MSV000088606 (https://massive.ucsd.edu/ProteoSAFe/dataset.jsp?accession=MSV000088606). Reference MS/MS spectra of isolated compounds were deposited in the GNPS public spectral library (CCMSLIB00009918413, CCMSLIB00009918414, CCMSLIB00009918415, CCMSLIB00009918416, CCMSLIB00009918417, CCMSLIB00009918418, CCMSLIB00009918419, CCMSLIB00009918420, CCMSLIB00009918421, CCMSLIB00009918424, CCMSLIB00009918426, CCMSLIB00009918427, CCMSLIB00009918428, CCMSLIB00009918429, CCMSLIB00009918430, CCMSLIB00009918431, CCMSLIB00009918432, CCMSLIB00009918433). All occurrences will be added to Wikidata upon publication.

All spectra were searched against a custom version of the ISDB-LOTUS database,[30,31,64] completed with the *Dictionary of Natural Products* (DNP v30.1) using spectral_lib_matcher (https://github.com/mandelbrot-project/spectral_lib_matcher). All candidates with less than 0.02 Da deviation from expected mass were kept. Annotations were then completed and reweighted using an updated version (https://github.com/taxonomicallyinformedannotation/tima-r) of the published taxonomically informed scoring[16] and the same custom LOTUS-DNP library. MS1 annotation complementation was performed with 10 ppm tolerance and 0.05 min for adducts. Allowed adducts were: $[M+3H]^{3+}$, $[M+2H+Na]^{3+}$, $[M+H+2Na]^{3+}$, $[M+3Na]^{3+}$, $[M+2H]^{2+}$, $[M+2H+NH_3]^{2+}$, $[M+H+Na]^{2+}$, $[M+H+K]^{2+}$, $[M+2H+CH_3CN]^{2+}$, $[M+2Na]^{2+}$, $[M+2H+2CH_3CN]^{2+}$, $[M+2H+3CH_3CN]^{2+}$, $[M+H]^{+}$, $[M+NH_3]^{+}$, $[M+CH_3CN]^{+}$, $[M+CH_3OH]^{+}$, $[M+K]^{+}$, $[M+H+CH_3CN]^{+}$, $[M-H+2Na]^{+}$, $[M+C_2H_7N]^{+}$, $[M+Na+CH_3CN]^{+}$, $[M-H+2K]^{+}$, $[M+H+2CH_3CN]^{+}$, $[2M+H]^{+}$, $[2M+H+NH_3]^{+}$, $[2M+Na]^{+}$, $[2M+K]^{+}$, $[2M+H+CH_3CN]^{+}$, $[2M+Na+CH_3CN]^{+}$. Initial candidates were set to 50 and weighted candidates to 3. Spectral weight was set to 0.333, chemical weight to 0.167, and biological weight to 0.500. Chemical and biological scores were attributed to rank/n(ranks), respectively.

The features bioactivity score was calculated as the mean of the NPIs of the fractions attributed to the feature, multiplied by the feature abundance in the given fractions.

Outputs were finally visualized using Cytoscape 3.9.0 software.[65] The color and the size of the nodes were adapted to different parameters, depending on the layouts.

Extraction and Isolation, *Hyptis brevipes*. Ground aerial parts of *H. brevipes* (350 g) were macerated (5 × 5 L EtOAc). The extract was dried under reduced pressure and freeze-dried to afford 10.9 g of dry residue. The extract was fractionated by flash chromatography on silica gel (7 × 40cm i.d.) utilizing a gradient of EtOAc in *n*-hexane [0−20% (0−20 min), 20−40% (20−75 min), 40−100% (75−300 min), 100% EtOAc (300−330 min), and a final wash with 100% MeOH for 30 min; flow rate 30 mL/min; sample introduction via dry load (10.2 g extract absorbed on 40 g silica gel 65−200 μm)]. Fractions (22 mL) were collected and pooled based on their TLC (100% EtOAc) patterns to 17 main fractions F1−F17: F1 (waste, 70.3 mg), F2 (1−60; 1.1 g), F3 (61−104; 814.8 mg), F4 (105−139; 951.5 mg); F5 (140−169; 324. 6 mg), F6 (170−196; 246.3 mg), F7 (197−206; 79.2 mg), F8 (207−225; 232.5 mg), F9 (226−245; 1.2 g), F10 (246−257; 125.5 mg), F11 (258−266; 238.3 mg), F12 (267−274; 89.5 mg), F13 (275−297; 123.9 mg), F14 (298−320; 371.5 mg), F15 (321−339; 86.5 mg), F16 (340−369; 101.4 mg), F17 (370−410 + wash; 4.2 g).

Fractions F10, F11 and F15 were submitted to preparative RP-HPLC with a gradient of 10−100% CH_3CN (solvents containing 0.1% FA) over 30 min. Several injections of F10 (125 mg) afforded **7** (12.4 mg, t_R 15.9 min), F11 (238 mg) afforded subfraction P3 (39.3 mg, t_R 18.3 min), and F15 (86 mg) afforded subfraction B2 (22.3 mg, t_R 15.4 min). P3 was further separated by semipreparative RP-HPLC using 40% CH_3CN (t_R 9.6 min). Further separation with 52% MeOH (both solvents containing 0.1% FA) provided **1** (16.6 mg, t_R 27.4 min) and **2** (3.2 mg, t_R 23.5 min). B2 was submitted to semipreparative HPLC with a gradient 40−70% MeOH over 30 min to afford fraction C2 (13.3 mg, t_R 13.5 min). Compounds **4** (1.7 mg, t_R 18.0 min) and **5** (12.1 mg, t_R 16.3 min) were isolated by RP-HPLC of C2 with 29% CH_3CN (solvents containing 0.1% FA). F17 (4.2 g) was submitted to preparative RP-HPLC with a gradient of 20−70% CH_3CN (both containing 0.1% FA) over 45 min, to afford fraction T2 (18.4 mg, t_R 13.7 min). T2 was submitted to semipreparative HPLC with 25% CH_3CN (solvents containing 0.1% FA) to afford **6** (0.8 mg, t_R 14.6 min) and **3** (11 mg, t_R 17.1 min).

Extraction and Isolation, *Hyptis brachiata*. Ground aerial parts of *H. brachiata* (712 g) were percolated with EtOAc (9 L), followed by MeOH (17 L), at a flow rate of 5 mL/min. Evaporation under reduced pressure afforded 9.4 g of EtOAc and 27.4 g of MeOH extract. The EtOAc extract (9.3 g) was prepared for dry loading

https://doi.org/10.1021/acs.jnatprod.2c00146
J. Nat. Prod. XXXX, XXX, XXX−XXX

adsorbed on 35 g silica gel, and fractionated by flash chromatography on a silica column (7 × 46 cm, i.d.) with a gradient of EtOAc in *n*-hexane [2% (0−10 min), 2−70% (10−450 min), 70−100% (450−570 min), 100% (570−615 min)], followed by MeOH in EtOAc [(0−50% (615−735 min), 50−100% (8735−750 min), 100% (750−810 min); flow rate of 20 mL/min]. A total of 808 fractions were collected and combined based on TLC analysis [*n*-hexane-EtOAc (7:3 for fractions 1−264, 1:1 for fractions 265−598, 3:7 for fractions 598−688), EtOAc-MeOH (8:2 for fractions 655−808)] to 28 fractions (F1−F28). Further separation of F21 (249.7 mg) by preparative HPLC with a gradient of 5−100% CH_3CN in water (both containing 0.1% FA) in 30 min gave 21 fractions F21−1 to F21−21. Fraction F21−13 (17.9 mg, t_R 19.0 min) was further purified by semipreparative HPLC using a gradient of 30−60% CH_3CN in water (both containing 0.1% formic acid) in 30 min to yield **8** (8.9 mg, t_R 15.9 min).

Extraction and Isolation, *Artemisia argyi*. Fraction N (900 mg) of an *A. argyi* whole plant EtOAc extract from a previous study[50] was fractionated by flash chromatography on silica gel (3.5 × 45 cm i.d.). Sample was introduced as dry load (900 mg sample adsorbed on 2.7 g silica gel). The column was eluted with a gradient of MeOH in $CHCl_3$ [1% MeOH (0−40 min), 1−10% (40−120 min), 10−12.5% (120−135 min), 12.5−20% (135−155 min), 20−100% (155−165 min), 100% (165−200 min)]. Fractions were combined based on TLC analysis ($CHCl_3$-MeOH, 95:5) to fractions N_A to N_J. Fraction N_A (46.9 mg) was submitted to semipreparative RP-HPLC with 38% CH_3CN + 0.1% FA, yielding **11** (1.5 mg, t_R 16.0 min) and **12** (1.8 mg, t_R 21.5 min). Fraction N_F (104.7 mg) was submitted to semipreparative RP-HPLC with 30% CH_3CN + 0.1% FA, to afford compounds **10** (35 mg, t_R 15.5 min) and **9** (3.9 mg, t_R 17.5 min).

*Brevipolide A (**1**).* Colorless oil; UV (MeOH) λ_{max} (log ε) 207 (4.3), 226 (4.1), 315 (4.4) nm; ECD (*c* 0.31 mM, MeOH, 1 mm path length) λ_{max} ($\Delta\varepsilon$) 231 (−1.26), 255 (+4.02), 308 (+6.94); ^{1}H and ^{13}C NMR, see Table S4, Supporting Information; HRESIMS *m*/*z* 429.1541 $[M + H]^+$ (calcd for $C_{23}H_{25}O_8^+$, 429.1544). SMILES: CC(C(=O)[C@H]1C[C@@H]1[C@@H]([C@H]2CC=CC(=O)O2)OC(=O)C)OC(=O)/C=C/C3=CC=C(C=C3)O. InChIKey: HEYOPWSFHOXZQH-ZEEHAMELSA-N

*Brevipolide B (**2**).* Colorless oil; UV (MeOH) λ_{max} (log ε) 207 (4.4, sh), 227 (4.1), 309 (4.1, sh) nm; ECD (*c* 0.31 mM, MeOH, 1 mm path length) λ_{max} ($\Delta\varepsilon$) 229 (−0.82), 260 (+2.94), 317 (−3.92); ^{1}H and ^{13}C NMR, see Table S4, Supporting Information; HRESIMS *m*/*z* 429.1538 $[M + H]^+$ (calcd for $C_{23}H_{25}O_8^+$, 429.1544). SMILES: CC(C(=O)[C@H]1C[C@@H]1[C@@H]([C@H]2CC=CC(=O)O2)OC(=O)C)OC(=O)/C=C\C3=CC=C(C=C3)O. InChIKey: HEYOPWSFHOXZQH-SOBDBXMASA-N

*Brevipolide C (**3**).* Pale yellow transparent oil; UV (MeOH) λ_{max} (log ε) 216 (4.3, sh), 245 (4.0), 302 (4.1, sh), 332 (4.3) nm; ECD (*c* 0.33 mM, MeOH, 1 mm path length) λ_{max} ($\Delta\varepsilon$) 229 (−1.33), 260 (+3.09), 301 (+4.65), 328 (+3.06); ^{1}H and ^{13}C NMR, see Table S5, Supporting Information; HRESIMS *m*/*z* 403.1389 $[M + H]^+$ (calcd for $C_{21}H_{23}O_8^+$, 403.1387). SMILES: CC(C(=O)[C@H]1C[C@@H]1[C@@H]([C@H]2CC=CC(=O)O2)O)OC(=O)/C=C/C3=CC(=C(C=C3)O)O. InChIKey: PMVFYHVSZOZDAN-WJWNCLPLSA-N

*Brevipolide F (**4**).* Colorless oil; UV (MeOH) λ_{max} (log ε) 207 (4.4), 226 (4.1), 314 (4.3) nm; ECD (*c* 0.34 mM, MeOH, 1 mm path length) λ_{max} ($\Delta\varepsilon$) 228 (−0.94), 258 (+4.27), 321 (−2.78); ^{1}H and ^{13}C NMR, see Table S6, Supporting Information; HRESIMS *m*/*z* 387.1408 $[M + H]^+$ (calcd for $C_{21}H_{23}O_7^+$, 387.1438). SMILES: CC(C(=O)[C@H]1C[C@@H]1[C@@H]([C@H]2CC=CC(=O)O2)O)OC(=O)/C=C\C3=CC=C(C=C3)O. InChIKey: BJDMHAYLPGRUFH-BSGJGGAISA-N

*Brevipolide G (**5**).* Colorless oil; UV (MeOH) λ_{max} (log ε) 209 (4.3, sh), 227 (4.1, sh), 315 (4.4) nm; ECD (*c* 0.34 mM, MeOH, 1 mm path length) λ_{max} ($\Delta\varepsilon$) 230 (−2.75), 256 (+3.15), 308 (+6.24); ^{1}H and ^{13}C NMR, see Table S6, Supporting Information; HRESIMS *m*/*z* 387.1404 $[M + H]^+$ (calcd for $C_{21}H_{23}O_7^+$, 387.1438). SMILES: C[C@@H](C(=O)[C@H]1C[C@@H]1[C@@H]([C@H]-2CC=CC(=O)O2)O)OC(=O)/C=C/C3=CC=C(C=C3)O. InChIKey: BJDMHAYLPGRUFH-HIELJHRRSA-N

*3,7-Dimethylquercetagetin (**6**).* Yellow amorphous solid; ^{1}H and ^{13}C NMR, see Table S7, Supporting Information; ESIMS 347 *m*/*z* $[M + H]^+$. SMILES: COC1=C(C(=C2C(=C1)OC(=C(C2=O)OC)-C3=CC(=C(C=C3)O)O)O)O. InChIKey: WGWGXVOAFMLMJZ-UHFFFAOYSA-N

*Chrysosplenol C (**7**).* Yellow amorphous solid; ^{1}H and ^{13}C NMR, see Table S7, Supporting Information; HRESIMS *m*/*z* 361.0920 $[M + H]^+$ (calcd for $C_{18}H_{17}O_8^+$, 361.0918). SMILES: COC1=C(C=CC-(=C1)C2=C(C(=O)C3=C(C(=C(C=C3O2)OC)O)O)OC)O. InChIKey: QQBSPLCHDUCBNM-UHFFFAOYSA-N

*Sideritoflavone (**8**).* Yellow amorphous solid, ^{1}H and ^{13}C NMR, see Table S8, Supporting Information; ESIMS 361 *m*/*z* $[M + H]^+$. SMILES: COC1=C(C(=C2C(=C1O)C(=O)C=C(O2)C3=CC-(=C(C=C3)O)O)OC)OC. InChIKey: UWNUJPINKMRKKR-UHFFFAOYSA-N

*6-Methoxytricin (**9**).* Yellow amorphous solid, ^{1}H and ^{13}C NMR, see Table S9, Supporting Information; HRESIMS *m*/*z* 361.0911 $[M + H]^+$ (calcd for $C_{18}H_{17}O_8^+$, 361.0918). SMILES: COC1=CC(=CC-(=C1O)OC)C2=CC(=O)C3=C(O2)C=C(C(=C3O)OC)O. InChIKey: BVRHGBHZAQNORL-UHFFFAOYSA-N

*Jaceosidin (**10**).* Yellow solid; ^{1}H and ^{13}C NMR, see Table S9, Supporting Information; HRESIMS *m*/*z* 331.0807 $[M + H]^+$ (calcd for $C_{17}H_{15}O_7^+$, 331.0812). SMILES: COC1=C(C=CC(=C1)C2=CC-(=O)C3=C(O2)C=C(C(=C3O)OC)O)O. InChIKey: GLAAQZFBFGEBPS-UHFFFAOYSA-N

*Eupatilin (**11**).* Yellow solid; ^{1}H and ^{13}C NMR, see Table S9, Supporting Information; ESIMS 345 *m*/*z* $[M + H]^+$. SMILES: COC1=C(C=C(C=C1)C2=CC(=O)C3=C(O2)C=C(C(=C3O)-OC)O)OC. InChIKey: DRRWBCNQOKKKOL-UHFFFAOYSA-N

*Chrysosplenetin (**12**).* Yellow solid; ^{1}H and ^{13}C NMR, see Table S9, Supporting Information; HRESIMS *m*/*z* 375.1084 $[M + H]^+$ (calcd for $C_{19}H_{19}O_8^+$, 375.1074). SMILES: COC1=C(C=CC(=C1)-C2=C(C(=O)C3=C(C(=C(C=C3O2)OC)OC)O)O)OC)O. InChIKey: NBVTYGIYKCPHQN-UHFFFAOYSA-N

Calculation of ECD Spectra. Conformational analysis was performed with Schrödinger MacroModel 11.0 (Schrödinger, LLC, New York) employing the OPLS2005 (optimized potential for liquid simulations) force field in H_2O for geometrical optimization in two steps. In the first step, a global minimum was searched using 30,000 steps, in the second step, the global minimum was used for a conformational search (10,000 steps) choosing ten conformers to be subjected to geometrical optimization and energy calculation applying DFT at the CAM-B3LYP/Def2SVP level of theory, employing the SCRF method and the CPMC model for solvation in MeOH with the Gaussian 09 program package.[66] Excitation energy (denoted by wavelength in nm), rotator strength (R_{str}), dipole velocity (R_{vel}), and dipole length (R_{len}) were calculated in MeOH by TD-DFT at the same level of theory. ECD curves were obtained on the basis of rotator strengths with a half-band of 0.25 eV using SpecDis v1.7.[67]

High-Content Assay. A high-content assay (HCA) was performed as previously described.[23] In brief, patient-derived MM121224 cells[25] were transfected to genetically encoding H2B-mTurquoise, ERK- and AKT-KTRs. For the experiments, cells were seeded in 96-well plates and incubated with extracts, fractions, or pure compounds. Afterward, they were fixed and imaged with a HCS microscope. A computer vision approach was used to automatically segment each cell, and extract a ratio of cytosol over nuclear ratio indicative of ERK or AKT activity. The isolated compounds were tested at eight different concentrations starting at 200 μM to 1.56 μM (97 μM to 0.8 μM for **8**).

■ ASSOCIATED CONTENT

Supporting Information

The Supporting Information is available free of charge at https://pubs.acs.org/doi/10.1021/acs.jnatprod.2c00146.

^{1}H and ^{13}C NMR spectra for all compounds, additional HPLC-based activity profiles, ECD spectra, chromato-

https://doi.org/10.1021/acs.jnatprod.2c00146
J. Nat. Prod. XXXX, XXX, XXX−XXX

grams of prioritized m/z, annotation tables of the two prioritized clusters, and concentration−response curve of all compounds (PDF)

AUTHOR INFORMATION

Corresponding Author

Eliane Garo − *Division of Pharmaceutical Biology, Department of Pharmaceutical Sciences, University of Basel, 4056 Basel, Switzerland;* orcid.org/0000-0002-3497-2524; Email: eliane.garo@unibas.ch

Authors

Tanja Hell − *Division of Pharmaceutical Biology, Department of Pharmaceutical Sciences, University of Basel, 4056 Basel, Switzerland;* orcid.org/0000-0002-8867-2412

Adriano Rutz − *School of Pharmaceutical Sciences, University of Geneva, CH-1211 Geneva, Switzerland; Institute of Pharmaceutical Sciences of Western Switzerland, University of Geneva, CH-1211 Geneva, Switzerland;* orcid.org/0000-0003-0443-9902

Lara Dürr − *Division of Pharmaceutical Biology, Department of Pharmaceutical Sciences, University of Basel, 4056 Basel, Switzerland;* orcid.org/0000-0001-6551-1854

Maciej Dobrzyński − *Institute of Cell Biology, University of Bern, 3012 Bern, Switzerland;* orcid.org/0000-0002-0208-7758

Jakob K. Reinhardt − *Division of Pharmaceutical Biology, Department of Pharmaceutical Sciences, University of Basel, 4056 Basel, Switzerland;* orcid.org/0000-0002-8675-1029

Timo Lehner − *Division of Pharmaceutical Biology, Department of Pharmaceutical Sciences, University of Basel, 4056 Basel, Switzerland*

Morris Keller − *Division of Pharmaceutical Biology, Department of Pharmaceutical Sciences, University of Basel, 4056 Basel, Switzerland;* orcid.org/0000-0002-4316-6591

Anika John − *Institute of Cell Biology, University of Bern, 3012 Bern, Switzerland*

[¶]Mahabir Gupta − *Center for Pharmacognostic Research and Panamanian Flora, Faculty of Pharmacy, University of Panama, Panama City 0824, Republic of Panama*

Olivier Pertz − *Institute of Cell Biology, University of Bern, 3012 Bern, Switzerland*

Matthias Hamburger − *Division of Pharmaceutical Biology, Department of Pharmaceutical Sciences, University of Basel, 4056 Basel, Switzerland;* orcid.org/0000-0001-9331-273X

Jean-Luc Wolfender − *School of Pharmaceutical Sciences, University of Geneva, CH-1211 Geneva, Switzerland; Institute of Pharmaceutical Sciences of Western Switzerland, University of Geneva, CH-1211 Geneva, Switzerland;* orcid.org/0000-0002-0125-952X

Complete contact information is available at: https://pubs.acs.org/10.1021/acs.jnatprod.2c00146

Author Contributions

[‡]T.H. and A.R. contributed equally to this work.

Notes

The authors declare no competing financial interest.

[¶]Deceased on December 14, 2020.

ACKNOWLEDGMENTS

We thank Mitchell Levesque (University Hospital of Zurich) for providing the MM121224 cell line, and Albert Mattei (Institute of Cell Biology, University of Bern) for transfecting them with the KTRs. We thank Pascal Lorentz and the DBM Microscopy Core Facility (Department of Biomedicine, University of Basel) for access to the HCS microscope and for technical support. We acknowledge Alex Espinosa (botanist at CILORPAN) for the identification of the Panamanian plants. ECD spectra were measured at the Biophysics Facility, Biozentrum, University of Basel. Funding was provided by grants from the Swiss National Science Foundation (to Matthias Hamburger and Olivier Pertz, 205321-176008, and to Jean-Luc Wolfender Sinergia grant CRSII5_189921) and from the Swiss Cancer League (KFS-3727-08-2015; Olivier Pertz).

REFERENCES

(1) Butler, M. S. *J. Nat. Prod.* **2004**, *67*, 2141−2153.
(2) Koehn, F. E.; Carter, G. T. *Nat. Rev. Drug Discov* **2005**, *4*, 206−220.
(3) Wolfender, J.-L.; Litaudon, M.; Touboul, D.; Queiroz, E. F. *Nat. Prod. Rep.* **2019**, *36*, 855−868.
(4) Butler, M.; Fontaine, F.; Cooper, M. *Planta Med.* **2014**, *80*, 1161−1170.
(5) Wilson, B. A. P.; Thornburg, C. C.; Henrich, C. J.; Grkovic, T.; O'Keefe, B. R. *Nat. Prod. Rep.* **2020**, *37*, 893−918.
(6) Wolfender, J.-L.; Marti, G.; Thomas, A.; Bertrand, S. *Journal of Chromatography A* **2015**, *1382*, 136−164.
(7) Molinski, T. F. *Nat. Prod. Rep.* **2010**, *27*, 321.
(8) Kongstad, K. T.; Özdemir, C.; Barzak, A.; Wubshet, S. G.; Staerk, D. *J. Agric. Food Chem.* **2015**, *63*, 2257−2263.
(9) Wang, M.; Carver, J. J.; Phelan, V. V.; Sanchez, L. M.; Garg, N.; Peng, Y.; Nguyen, D. D.; Watrous, J.; Kapono, C. A.; Luzzatto-Knaan, T.; Porto, C.; Bouslimani, A.; Melnik, A. V.; Meehan, M. J.; Liu, W.-T.; Crüsemann, M.; Boudreau, P. D.; Esquenazi, E.; Sandoval-Calderón, M.; Kersten, R. D.; Pace, L. A.; Quinn, R. A.; Duncan, K. R.; Hsu, C.-C.; Floros, D. J.; Gavilan, R. G.; Kleigrewe, K.; Northen, T.; Dutton, R. J.; Parrot, D.; Carlson, E. E.; Aigle, B.; Michelsen, C. F.; Jelsbak, L.; Sohlenkamp, C.; Pevzner, P.; Edlund, A.; McLean, J.; Piel, J.; Murphy, B. T.; Gerwick, L.; Liaw, C.-C.; Yang, Y.-L.; Humpf, H.-U.; Maansson, M.; Keyzers, R. A.; Sims, A. C.; Johnson, A. R.; Sidebottom, A. M.; Sedio, B. E.; Klitgaard, A.; Larson, C. B.; Boya P, C. A.; Torres-Mendoza, D.; Gonzalez, D. J.; Silva, D. B.; Marques, L. M.; Demarque, D. P.; Pociute, E.; O'Neill, E. C.; Briand, E.; Helfrich, E. J. N.; Granatosky, E. A.; Glukhov, E.; Ryffel, F.; Houson, H.; Mohimani, H.; Kharbush, J. J.; Zeng, Y.; Vorholt, J. A.; Kurita, K. L.; Charusanti, P.; McPhail, K. L.; Nielsen, K. F.; Vuong, L.; Elfeki, M.; Traxler, M. F.; Engene, N.; Koyama, N.; Vining, O. B.; Baric, R.; Silva, R. R.; Mascuch, S. J.; Tomasi, S.; Jenkins, S.; Macherla, V.; Hoffman, T.; Agarwal, V.; Williams, P. G.; Dai, J.; Neupane, R.; Gurr, J.; Rodríguez, A. M. C.; Lamsa, A.; Zhang, C.; Dorrestein, K.; Duggan, B. M.; Almaliti, J.; Allard, P.-M.; Phapale, P.; Nothias, L.-F.; Alexandrov, T.; Litaudon, M.; Wolfender, J.-L.; Kyle, J. E.; Metz, T. O.; Peryea, T.; Nguyen, D.-T.; VanLeer, D.; Shinn, P.; Jadhav, A.; Müller, R.; Waters, K. M.; Shi, W.; Liu, X.; Zhang, L.; Knight, R.; Jensen, P. R.; Palsson, B. Ø.; Pogliano, K.; Linington, R. G.; Gutiérrez, M.; Lopes, N. P.; Gerwick, W. H.; Moore, B. S.; Dorrestein, P. C.; Bandeira, N. *Nat. Biotechnol.* **2016**, *34*, 828−837.
(10) Quinn, R. A.; Nothias, L.-F.; Vining, O.; Meehan, M.; Esquenazi, E.; Dorrestein, P. C. *Trends Pharmacol. Sci.* **2017**, *38*, 143−154.
(11) Cabral, R. S.; Allard, P.-M.; Marcourt, L.; Young, M. C. M.; Queiroz, E. F.; Wolfender, J.-L. *J. Nat. Prod.* **2016**, *79*, 2270−2278.
(12) Beniddir, M. A.; Kang, K. B.; Genta-Jouve, G.; Huber, F.; Rogers, S.; van der Hooft, J. J. J. *Nat. Prod. Rep.* **2021**, *38*, 1967−1993.

(13) Kim, H. W.; Wang, M.; Leber, C. A.; Nothias, L.-F.; Reher, R.; Kang, K. B.; van der Hooft, J. J. J.; Dorrestein, P. C.; Gerwick, W. H.; Cottrell, G. W. *J. Nat. Prod.* **2021**, *84*, 2795−2807.
(14) Dührkop, K.; Nothias, L.-F.; Fleischauer, M.; Reher, R.; Ludwig, M.; Hoffmann, M. A.; Petras, D.; Gerwick, W. H.; Rousu, J.; Dorrestein, P. C.; Böcker, S. *Nat. Biotechnol.* **2021**, *39*, 462−471.
(15) Hoffmann, M. A.; Nothias, L.-F.; Ludwig, M.; Fleischauer, M.; Gentry, E. C.; Witting, M.; Dorrestein, P. C.; Dührkop, K.; Böcker, S. *Nat. Biotechnol.* **2022**, *40*, 411−421.
(16) Rutz, A.; Dounoue-Kubo, M.; Ollivier, S.; Bisson, J.; Bagheri, M.; Saesong, T.; Ebrahimi, S. N.; Ingkaninan, K.; Wolfender, J.-L.; Allard, P.-M. *Front. Plant Sci.* **2019**, *10*, 1329.
(17) Hanke, W.; Patt, J.; Alenfelder, J.; Voss, J. H.; Zdouc, M. M.; Kehraus, S.; Kim, J. B.; Grujičić, G. V.; Namasivayam, V.; Reher, R.; Müller, C. E.; Kostenis, E.; Crüsemann, M.; König, G. M. *J. Nat. Prod.* **2021**, *84*, 1941−1953.
(18) Bracegirdle, J.; Hou, P.; Nowak, V. V.; Ackerley, D. F.; Keyzers, R. A.; Owen, J. G. *J. Nat. Prod.* **2021**, *84*, 2536−2543.
(19) Olivon, F.; Remy, S.; Grelier, G.; Apel, C.; Eydoux, C.; Guillemot, J.-C.; Neyts, J.; Delang, L.; Touboul, D.; Roussi, F.; Litaudon, M. *J. Nat. Prod.* **2019**, *82*, 330−340.
(20) Wang, R.; Liu, Y.; Zhou, H.; Chen, Y.; Wang, J.; Zhang, X.; Yu, R.; Liang, X. *Journal of Chromatography A* **2020**, *1616*, 460779.
(21) Nothias, L.-F.; Nothias-Esposito, M.; da Silva, R.; Wang, M.; Protsyuk, I.; Zhang, Z.; Sarvepalli, A.; Leyssen, P.; Touboul, D.; Costa, J.; Paolini, J.; Alexandrov, T.; Litaudon, M.; Dorrestein, P. C. *J. Nat. Prod.* **2018**, *81*, 758−767.
(22) Potterat, O.; Hamburger, M. *Planta Med.* **2014**, *80*, 1171−1181.
(23) Dürr, L.; Hell, T.; Dobrzyński, M.; Mattei, A.; John, A.; Augsburger, N.; Bradanini, G.; Reinhardt, J. K.; Rossberg, F.; Drobnjakovic, M.; Gupta, M. P.; Hamburger, M.; Pertz, O.; Garo, E. *J. Nat. Prod.* **2022**, *85*, 1006−1017.
(24) Wink, M. *Phytochemistry* **2003**, *64*, 3−19.
(25) Raaijmakers, M. I. G.; Widmer, D. S.; Narechania, A.; Eichhoff, O.; Freiberger, S. N.; Wenzina, J.; Cheng, P. F.; Mihic-Probst, D.; Desalle, R.; Dummer, R.; Levesque, M. P. *Oncotarget* **2016**, *7*, 77163−77174.
(26) Maryu, G.; Matsuda, M.; Aoki, K. *Cell Struct. Funct.* **2016**, *41*, 81−92.
(27) Regot, S.; Hughey, J. J.; Bajar, B. T.; Carrasco, S.; Covert, M. W. *Cell* **2014**, *157*, 1724−1734.
(28) Guillarme, D.; Nguyen, D. T. T.; Rudaz, S.; Veuthey, J.-L. *Eur. J. Pharm. Biopharm.* **2008**, *68*, 430−440.
(29) Schmid, R.; Petras, D.; Nothias, L.-F.; Wang, M.; Aron, A. T.; Jagels, A.; Tsugawa, H.; Rainer, J.; Garcia-Aloy, M.; Dührkop, K.; Korf, A.; Pluskal, T.; Kameník, Z.; Jarmusch, A. K.; Caraballo-Rodríguez, A. M.; Weldon, K. C.; Nothias-Esposito, M.; Aksenov, A. A.; Bauermeister, A.; Albarracin Orio, A.; Grundmann, C. O.; Vargas, F.; Koester, I.; Gauglitz, J. M.; Gentry, E. C.; Hövelmann, Y.; Kalinina, S. A.; Pendergraft, M. A.; Panitchpakdi, M.; Tehan, R.; Le Gouellec, A.; Aleti, G.; Mannochio Russo, H.; Arndt, B.; Hübner, F.; Hayen, H.; Zhi, H.; Raffatellu, M.; Prather, K. A.; Aluwihare, L. I.; Böcker, S.; McPhail, K. L.; Humpf, H.-U.; Karst, U.; Dorrestein, P. C. *Nat. Commun.* **2021**, *12*, 3832.
(30) Allard, P.-M.; Bisson, J.; Rutz, A. *Zenodo*, **2021**. DOI: 10.5281/zenodo.5607185.
(31) Rutz, A.; Sorokina, M.; Galgonek, J.; Mietchen, D.; Willighagen, E.; Gaudry, A.; Graham, J. G.; Stephan, R.; Page, R.; Vondrášek, J.; Steinbeck, C.; Pauli, G. F.; Wolfender, J.-L.; Bisson, J.; Allard, P.-M. *eLife* **2022**. DOI: 10.7554/eLife.70780.
(32) Deng, Y.; Balunas, M. J.; Kim, J.-A.; Lantvit, D. D.; Chin, Y.-W.; Chai, H.; Sugiarso, S.; Kardono, L. B. S.; Fong, H. H. S.; Pezzuto, J. M.; Swanson, S. M.; Carcache de Blanco, E. J.; Kinghorn, A. D. *J. Nat. Prod.* **2009**, *72*, 1165−1169.
(33) Suárez-Ortiz, G. A.; Cerda-García-Rojas, C. M.; Hernández-Rojas, A.; Pereda-Miranda, R. *J. Nat. Prod.* **2013**, *76*, 72−78.
(34) Suárez-Ortiz, G. A.; Cerda-García-Rojas, C. M.; Fragoso-Serrano, M.; Pereda-Miranda, R. *J. Nat. Prod.* **2017**, *80*, 181−189.
(35) Urones, J. G.; Marcos, I. S.; Diez, D.; Cubilla, L. *Phytochemistry* **1998**, *48*, 1035−1038.
(36) Yoshikawa, M.; Shimada, H.; Matsuda, H.; Yamahara, J.; Murakami, N. *Chem. Pharm. Bull.* **1996**, *44*, 1656−1662.
(37) Chemesova, I. I.; Boiko, É. V *Chem. Nat. Compd.* **1990**, *26*, 713−713.
(38) Jeong, M. A.; Lee, K. W.; Yoon, D.-Y.; Lee, H. J. *Ann. N.Y. Acad. Sci.* **2007**, *1095*, 458−466.
(39) Lee, H.-G.; Yu, K.-A.; Oh, W.-K.; Baeg, T.-W.; Oh, H.-C.; Ahn, J.-S.; Jang, W.-C.; Kim, J.-W.; Lim, J.-S.; Choe, Y.-K.; Yoon, D.-Y. *Journal of Ethnopharmacology* **2005**, *98*, 339−343.
(40) Nakasugi, T.; Nakashima, M.; Komai, K. *J. Agric. Food Chem.* **2000**, *48*, 3256−3266.
(41) Seo, J.-M.; Kang, H.-M.; Son, K.-H.; Kim, J. H.; Lee, C. W.; Kim, H. M.; Chang, S.-I.; Kwon, B.-M. *Planta med* **2003**, *69*, 218−222.
(42) Marco, J. A.; Barberá, O.; Sánchez-Parareda, J. *J. Nat. Prod.* **1987**, *50*, 774−775.
(43) Hegde, V. R.; Pu, H.; Patel, M.; Das, P. R.; Strizki, J.; Gullo, V. P.; Chou, C.-C.; Buevich, A. V.; Chan, T.-M. *Bioorg. Med. Chem. Lett.* **2004**, *14*, 5339−5342.
(44) Ulubelen, A.; Kerr, K. M.; Mabry, T. J. *Phytochemistry* **1980**, *19*, 1761−1766.
(45) Huong, D. T.; Kamperdick, C.; Sung, T. V. *J. Nat. Prod.* **2004**, *67*, 445−447.
(46) Li, M.-L.; Xu, L.-Y.; Li, Z.-L.; Qian, S.-H.; Qin, M.-J. *Chem. Nat. Compd.* **2014**, *50*, 124−125.
(47) Kuhnt, M.; Pröbstle, A.; Rimpler, H.; Bauer, R.; Heinrich, M. *Planta Med.* **1995**, *61*, 227−232.
(48) Novelo, M.; Cruz, J. G.; Hernández, L.; Pereda-Miranda, R.; Chai, H.; Mar, W.; Pezzuto, J. M. *J. Nat. Prod.* **1993**, *56*, 1728−1736.
(49) Kuhnt, M.; Rimpler, H.; Heinrich, M. *Phytochemistry* **1994**, *36*, 485−489.
(50) Reinhardt, J. K.; Klemd, A. M.; Danton, O.; De Mieri, M.; Smieško, M.; Huber, R.; Bürgi, T.; Gründemann, C.; Hamburger, M. *J. Nat. Prod.* **2019**, *82*, 1424−1433.
(51) Liu, Y.; Mabry, T. J. *Phytochemistry* **1981**, *20*, 309−311.
(52) Liu, Y.-L.; Mabry, T. J. *Phytochemistry* **1982**, *21*, 209−214.
(53) Bouzid, N.; Fouraste, I.; Voirin, B.; Favre-Bonvin, J.; Lebreton, P. *Phytochemistry* **1982**, *21*, 803−804.
(54) Martínez, V.; Barberá, O.; Sánchez-Parareda, J.; Alberto Marco, J. *Phytochemistry* **1987**, *26*, 2619−2624.
(55) Sheng, Y.-H.; Leu, W.-J.; Chen, C.-N.; Hsu, J.-L.; Liu, Y.-T.; Hsu, L.-C.; Hou, D.-R.; Guh, J.-H. *Molecules* **2020**, *25*, 2929.
(56) Son, J.; Lee, E.; Seo, S.; Lee, J.; Kim, J.; Kim, J.; Lee, K.; Lee, H. *Planta Med.* **2013**, *79*, 1009−1016.
(57) Han, H.-Y.; Kim, H. J.; Jeong, S.-H.; Kim, J.; Jeong, S.-H.; Kim, G. C.; Hwang, D.-S.; Kim, U.-K.; Ryu, M. H. *Evidence-Based Complementary and Alternative Medicine* **2018**, *2018*, 1−9.
(58) Dirimanov, S.; Högger, P. *Biomolecules* **2019**, *9*, 219.
(59) Vlahos, C. J.; Matter, W. F.; Hui, K. Y.; Brown, R. F. *J. Biol. Chem.* **1994**, *269*, 5241−5248.
(60) Bisson, J.; McAlpine, J. B.; Friesen, J. B.; Chen, S.-N.; Graham, J.; Pauli, G. F. *J. Med. Chem.* **2016**, *59*, 1671−1690.
(61) Hulstaert, N.; Shofstahl, J.; Sachsenberg, T.; Walzer, M.; Barsnes, H.; Martens, L.; Perez-Riverol, Y. *J. Proteome Res.* **2020**, *19*, 537−542.
(62) Myers, O. D.; Sumner, S. J.; Li, S.; Barnes, S.; Du, X. *Anal. Chem.* **2017**, *89*, 8689−8695.
(63) Horai, H.; Arita, M.; Kanaya, S.; Nihei, Y.; Ikeda, T.; Suwa, K.; Ojima, Y.; Tanaka, K.; Tanaka, S.; Aoshima, K.; Oda, Y.; Kakazu, Y.; Kusano, M.; Tohge, T.; Matsuda, F.; Sawada, Y.; Hirai, M. Y.; Nakanishi, H.; Ikeda, K.; Akimoto, N.; Maoka, T.; Takahashi, H.; Ara, T.; Sakurai, N.; Suzuki, H.; Shibata, D.; Neumann, S.; Iida, T.; Tanaka, K.; Funatsu, K.; Matsuura, F.; Soga, T.; Taguchi, R.; Saito, K.; Nishioka, T. *J. Mass Spectrom.* **2010**, *45*, 703−714.
(64) Allard, P.-M.; Péresse, T.; Bisson, J.; Gindro, K.; Marcourt, L.; Pham, V. C.; Roussi, F.; Litaudon, M.; Wolfender, J.-L. *Anal. Chem.* **2016**, *88*, 3317−3323.

https://doi.org/10.1021/acs.jnatprod.2c00146
J. Nat. Prod. XXXX, XXX, XXX−XXX

(65) Shannon, P.; Markiel, A.; Ozier, O.; Baliga, N. S.; Wang, J. T.; Ramage, D.; Amin, N.; Schwikowski, B.; Ideker, T. *Genome Res.* **2003**, *13*, 2498−2504.
(66) Frisch, M. J.; Trucks, G. W.; Schlegel, H. B.; Scuseria, G. E.; Robb, M. A.; Cheeseman, J. R.; Scalmani, G.; Barone, V.; Petersson, G. A.; Nakatsuji, H.; Li, X.; Caricato, M.; Marenich, A.; Bloino, J.; Janesko, B. G.; Gomperts, R.; Mennucci, B.; Hratchian, H. P.; Ortiz, J. V.; Izmaylov, A. F.; Sonnenberg, J. L.; Williams-Young, D.; Ding, F.; Lipparini, F.; Egidi, F.; Goings, J.; Peng, B.; Petrone, A.; Henderson, T.; Ranasinghe, D.; Zakrzewski, V. G.; Gao, J.; Rega, N.; Zheng, G.; Liang, W.; Hada, M.; Ehara, M.; Toyota, K.; Fukuda, R.; Hasegawa, J.; Ishida, M.; Nakajima, T.; Honda, Y.; Kitao, O.; Naka, H.; Vreven, T.; Throssell, K.; Montgomery, J. A.; Peralta, J. E.; Ogliaro, F.; Bearpark, M.; Heyd, J. J.; Brothers, E.; Kudin, K. N.; Staroverov, V. N.; Keith, T.; Kobayashi, R.; Normand, J.; Raghavachari, K.; Rendel, A.; Burant, J. C.; Iyengar, S. S.; Tomasi, J.; Cossi, M.; Millam, J. M.; Klene, M.; Adamo, C.; Cammi, R.; Ochterski, J. W.; Martin, R. L.; Morokuma, K.; Farkas, O.; Foresman, J. B.; Fox, D. J. *Gaussian 09*, Revision D.01; Gaussian, Inc.: Wallingford, CT, 2009
(67) Bruhn, T.; Schaumlöffel, A.; Hemberger, Y.; Bringmann, G. *Chirality* **2013**, *25*, 243−249.

https://doi.org/10.1021/acs.jnatprod.2c00146
J. Nat. Prod. XXXX, XXX, XXX−XXX